Physics of Fluids

RESEARCH ARTICLE | SEPTEMBER 28 2026

Effect of a magnetostatic field on laminar premixed hydrogen–air flames

Special Collection: Recent Advances in Hydrodynamic Instabilities

Tristan Lapaire ; Sofiane Al Kassar ; Antonio Attili ; Andrea Giusti

Check for updates

Physics of Fluids 38, 097505 (2026)
https://doi.org/10.1063/5.0347557

View Online
Export Citation

Articles You May Be Interested In

Distribution of thermoacoustic instability and nonlinear characteristics of partially premixed hydrogen flames

Physics of Fluids (September 2026)

Flame-head splitting and local compression under half-open confinement during premixed hydrogen–air propagation

AIP Advances (September 2026)

Experimental investigation of the effect of mechanical vibration on the laminar premixed flame

Physics of Fluids (August 2024)

02 October 2026 08:40:23

AIP Publishing

Physics of Fluids

Special Topics Open for Submissions

Learn More

AIP Publishing

Physics of Fluids ARTICLE pubs.aip.org/aip/pof

Effect of a magnetostatic field on laminar premixed hydrogen–air flames

Cite as: Phys. Fluids **38**, 097505 (2026); doi: 10.1063/5.0347557
Submitted: 10 June 2026 · Accepted: 4 September 2026 ·
Published Online: 28 September 2026

View Online Export Citation CrossMark

Tristan Lapaire,[1,a)] Sofiane Al Kassar,[2] Antonio Attili,[2] and Andrea Giusti[1]

AFFILIATIONS

[1]Department of Mechanical Engineering, Imperial College London, London, United Kingdom
[2]School of Engineering, Institute for Multiscale Thermofluids, The University of Edinburgh, Edinburgh, United Kingdom

Note: This paper is part of the Special Topic on Recent Advances in Hydrodynamic Instabilities.
[a)]**Author to whom correspondence should be addressed:** t.lapaire-lemoine@imperial.ac.uk

ABSTRACT

Magnetic fields have shown potential to affect flame characteristics. However, the mechanisms of interaction between a magnetic field and a flame are not fully understood. This paper investigates the effect of magnetic fields on premixed hydrogen–air flames that are prone to intrinsic instabilities, with a focus on the impact of magnetic forces on the flame behavior. The study is conducted using direct numerical simulations. Two flame conditions, both with an equivalence ratio of 0.5, are studied: one with reactants at atmospheric conditions and the other with reactants at high pressure and high temperature. Different configurations of the magnetic field are investigated, each characterized by different values of the gradient of the square of the magnetic field. In all configurations with a magnetic field, this gradient is oriented in the direction opposite to the velocity of the incoming reactants. Results show that the investigated magnetic fields can reduce the flame consumption speed through a reduction in flame area, an effect that is substantial for the atmospheric pressure case. Conversely, in the high-pressure case, no significant effects of the magnetic fields are observed. Analysis of the force contributions demonstrates that the change in the flame area is caused by the rotational component of the magnetic forces, which alter the vorticity of the flow such that the hydrodynamic instability tends to reduce. These forces, which require a gradient of magnetic susceptibility not aligned with the gradient of the magnetic field magnitude, are significant at atmospheric pressure, while they become negligible compared to the pressure gradient at high pressure. Ultimately, the results of this work indicate that magnetic forces have the potential to change the flame behavior, a mechanism that could be used for active control of flame characteristics.

© *2026 Author(s). All article content, except where otherwise noted, is licensed under a Creative Commons Attribution (CC BY) license (https://creativecommons.org/licenses/by/4.0/).* https://doi.org/10.1063/5.0347557

02 October 2026 08:40:23

I. INTRODUCTION

The transition to a low-carbon economy requires, among others, the identification of alternative energy carriers. Hydrogen, with its high specific energy and zero carbon emissions during combustion, is often presented as one of the most promising solutions to reduce emissions in power generation and in sectors that are difficult to electrify. Despite its potential, direct combustion of hydrogen still faces many challenges, which are mainly related to the high reactivity and high diffusivity of this fuel.[1] These characteristics of hydrogen make the combustion process more prone to instabilities, including an increased risk of flashback, possibly affecting the safety of the combustion system.[2]

In lean premixed hydrogen flames, combustion instabilities occur intrinsically. These instabilities appear to arise from two mechanisms. The first mechanism, usually referred to as hydrodynamic, or Darrieus–Landau, instability, originates from gas expansion across the flame front and results in a non-uniform flow velocity along the flame front, causing the growth of the flame front perturbations.[3–6] The second mechanism is related to thermodiffusive instability, which arises from the strong differential diffusion caused by the non-unity Lewis number of hydrogen, promoting the formation of small-scale cellular structures and cusps on the flame surface.[7–9] These complex flame front dynamics strongly modify the global flame properties,[7–10] with potential implications for the optimal and safe use of hydrogen combustion. Being able to control, or at least influence, these instabilities would therefore constitute a significant step toward the safe use of hydrogen in practical applications.

Various strategies have been proposed for the stabilization and control of hydrogen flames, including swirl[11] and bluff-body stabilization,[12] acoustic forcing,[13] plasma actuation,[14] and fuel staging.[15]

© Author(s) 2026

Studies involving these strategies have primarily targeted the global stabilization of the flame and the mitigation of thermoacoustic instabilities, while the investigation of the effect of external fields on the intrinsic instabilities of hydrogen flames remains comparatively unexplored. Among the various strategies to control the flame behavior, the use of magnetic fields has attracted increased attention. Magnetic fields offer a contactless approach to modify the flame characteristics through volumetric body forces resulting from the magnetization of species. The idea of such a control finds its origin in Faraday's pioneering work.[16] Since then, the effect of magnetic fields has been investigated in a number of laboratory flame configurations, including hydrogen flames.[17–19] Research findings demonstrate that a magnetic field can lead to changes in the flame shape and distribution of species.[17–20] Evidence from these studies suggests that these effects are primarily due to forces acting on paramagnetic species, in particular oxygen,[17,21–23] which necessarily require the presence of a non-uniform magnetic field,[24] while with a uniform magnetic field, effects on the flame are negligible.[25] It is important to note that these studies have mainly focused on the overall flame characteristics without providing a comprehensive analysis of the forces acting on the flame front and the mechanism of interaction between the magnetic field and the flame. In particular, the physical processes linking the magnetic forces to changes in flame dynamics, including the effects of magnetic forces on vortical structures, have not been fully clarified. In addition, there are no detailed studies on the possible effect of an external magnetic field on the intrinsic instabilities of premixed hydrogen flames.

This study aims to investigate the interaction between magnetic forces and the flame front in laminar premixed hydrogen–air flames, with a focus on the effects of the magnetic field on the dynamics of the flame, including intrinsic instabilities, and overall flame characteristics. The specific objectives of the work are to (i) investigate the impact of magnetic fields on the flame behavior for increasing strength of the magnetic forces; (ii) study the effect of ambient conditions on the response of the flame to magnetic fields; and (iii) identify the mechanism of interaction between magnetic forces and the flame front. To achieve these objectives, a premixed laminar flame with an equivalence ratio of 0.5 is investigated using direct numerical simulations (DNSs) under different pressure and temperature conditions and with different configurations of the magnetic field. Insights into the interaction between magnetic forces and flame dynamics are provided through the analysis of flow vorticity and the decomposition of the magnetic force into irrotational and rotational (i.e., solenoidal) components. This work should be regarded as a fundamental study that can assist in the interpretation of current experiments and numerical investigations, as well as guide the development of future experiments involving the study of intrinsic instabilities under magnetic fields.

II. METHODS

A. Configuration

The configuration investigated in this work is a two-dimensional domain, schematically shown in Fig. 1, which represents a premixed laminar hydrogen–air flame stabilized in a magnetic field. The Cartesian frame of reference used throughout the study has its origin at the center of the inlet boundary. The premixed reactants enter the domain at $x = 0$. The velocity of the reactants is imposed such that a

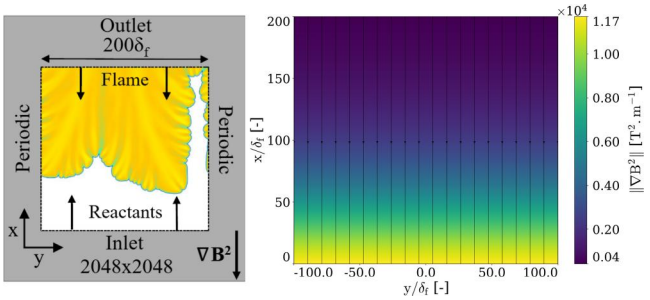


FIG. 1. Simulation domain and gradient of the square of the magnetic field for configuration (e). The domain is $200 \times 200\,\delta_f^2$, discretized on a 2048×2048 mesh ($\Delta x = \delta_f/10.24$). The reactants enter the domain in the positive x-direction; both the flame propagation and the gradient of the square of the magnetic field are oriented in the negative x-direction.

flame is stabilized (on average) in the middle of the domain (the flame tends to propagate in the negative x-direction). Two different reactant conditions are investigated in this work: a low-pressure case with reactants at atmospheric conditions (case 1), and a high-pressure condition with reactants at $T_i = 700$ K and $p = 20$ atm (case 2). The equivalence ratio is set to $\phi = 0.5$ in both cases, which ensures the presence of both Darrieus–Landau and thermodiffusive instabilities.[10] These conditions are summarized in Table I, which also reports the reference flame thickness, δ_f, and reference flame time, τ_f, associated with each condition, together with the main characteristics of the magnetic field configurations investigated here. Five different configurations of the magnetic field are studied, each characterized by a different gradient of the square of the magnetic field, $\nabla(B^2)$. For reference, the spatial distribution of $\nabla(B^2)$ for one of the configurations with a magnetic field is presented in Fig. 1 [the other configurations show a very similar orientation of $\nabla(B^2)$, apart from configuration (a), which has no magnetic field]. In all configurations with a magnetic field, $\nabla(B^2)$ is predominantly oriented in the negative x-direction, while the components of this gradient along y are negligible, which makes periodic boundaries applicable with very good approximation (note that, although negligible, these

TABLE I. Simulated cases and associated magnetic field configurations (see also Figs. 1 and 2 for more details regarding the investigated geometry and magnetic fields).

Case	T_i (K)	p (atm)	ϕ (-)	δ_f (m)	τ_f (s)
1.	298	1	0.5	4.57×10^{-4}	1.03×10^{-3}
2.	700	20	0.5	1.89×10^{-5}	1.43×10^{-5}

	$\|\nabla B^2\|$ ($T^2\,m^{-1}$)		
Config.	Inlet	Middle	Outlet
(a)	0	0	0
(b)	7.28×10^2	1.52×10^2	2.60×10^1
(c)	2.93×10^3	6.13×10^2	1.10×10^2
(d)	6.58×10^3	1.37×10^3	2.37×10^2
(e)	1.17×10^4	2.45×10^3	4.20×10^2

02 October 2026 08:40:23

© Author(s) 2026

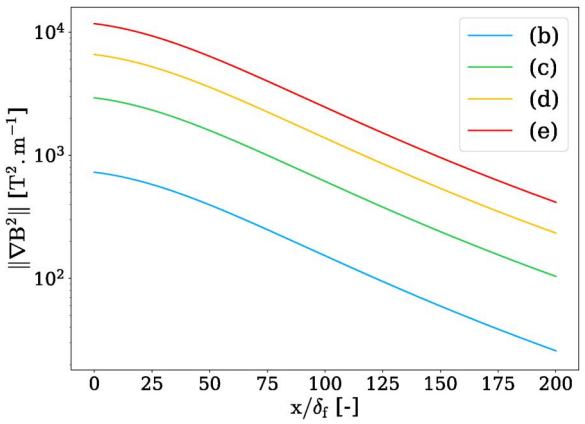


FIG. 2. Magnitude of $\nabla(B^2)$ as a function of x/δ_f for magnetic field configurations (b)–(e). This profile has been sampled at $y = 0$; the profile at different y locations is substantially the same. Given that the y-component of the magnetic field gradient is negligible, this profile represents the absolute value of the x-component of $\nabla(B^2)$.

components are not zero and the resulting field is symmetric with respect to the x axis). In addition, the x-component of the field is approximately uniform along the y-direction. The magnitude of $\nabla(B^2)$ as a function of x/δ_f for all configurations with non-zero magnetic field is shown in Fig. 2, which highlights the variation of the strength of the magnetic field gradient from the inlet to the outlet of the domain. These magnetostatic fields have been obtained using Magpylib,[26] which allows us to obtain physically consistent (i.e., divergence-free) magnetic fields. The various configurations were initially designed for the high pressure and temperature case (case 2) to represent magnetic fields that could be obtained with practical magnets, and then extended to case 1 by imposing the same magnetic field gradient in the scaled domain. Note that the obtained configurations have a magnitude of $\nabla(B^2)$ that decreases with increasing distance from the inlet boundary (see Table I). The average magnitude of $\nabla(B^2)$ increases from configuration (a) to (e). It should be noted that the magnetic field gradients obtained in configuration (e) are relatively high. Practical implementation of these gradients may require strong magnetic fields (e.g., generated by superconducting magnets) as well as arrays of magnets to obtain a sustained magnetic field gradient over a large space. The design of such configurations should be carefully evaluated in future work. Simulations of cases 1 and 2 were run for approximately 200 and 500 flame times, respectively, after the development of instabilities, which were obtained by initializing the simulations with perturbations.[27]

B. Governing equations and numerical methods

The various cases are numerically studied using direct numerical simulation (DNS). The unsteady reacting Navier–Stokes equations are solved in the low Mach number limit, with the mixture obeying the ideal gas law.[28] The transport equations for the species and temperature are solved using a finite-rate multistep chemical mechanism with nine species and 46 reactions.[29] The viscosity of the mixture is calculated with Wilke's formula.[30] The transport properties are evaluated using a mixture-averaged model based on Bird's expression.[31,32] The diffusive fluxes of the species are evaluated using the Hirschfelder and Curtis approximation,[33,34] with the thermodiffusive, or Soret, effect included using the Hirschfelder and Warnatz approximation.[35] The equations are solved with a semi-implicit finite difference code,[36] extensively used in previous work on reacting flows.[8,27,37] In this work, the code has been further developed through the addition of magnetic force terms to the momentum and temperature transport equations, as well as to the diffusion of species. The formulation of these equations with the additional body force terms can be found in Ref. 38. Spatial discretization of the convective terms in the species transport equations is performed using a third-order WENO scheme,[39] while a second-order scheme is used for the diffusion terms and the momentum equation. The Strang operator splitting is applied to the chemical source term, which is integrated with the stiff ODE solver CVODE.[40]

In this study, only the magnetization force is considered. This is expressed for each species k using the Kelvin force density model,[24] which, approximated to leading order using a linear medium assumption for the species, is given by

$$\mathbf{f}_k = \frac{\chi_k}{2\mu_0}\nabla(B^2), \tag{1}$$

where μ_0 is the magnetic permeability of free space and χ_k is the volume magnetic susceptibility of the kth species, which represents the magnetic response of a species to a magnetic field. Note that the susceptibility of diamagnetic species is orders of magnitude lower than the susceptibility of paramagnetic species. Therefore, in this study, the magnetic force is only taken into account for paramagnetic species. For each species, the value of χ_k mainly depends on the local temperature and species partial density and is expressed using the Curie law[41,42] as

$$\chi_k = \frac{\rho Y_k \mathcal{N}_A g_{L,k}^2 \mu_B^2 \mu_0 \mathcal{S}_k(\mathcal{S}_k+1)}{3W_k k_B T}, \tag{2}$$

where ρ and T are the local density and temperature of the mixture, respectively, $\mathcal{N}_A$ is the Avogadro number, Y_k is the mass fraction of species k, W_k is its molar mass, μ_B and k_B are the Bohr magneton and Boltzmann constant, respectively, $\mathcal{S}_k$ is the total quantum spin, and $g_{L,k}$ is the Landé g-factor,[43] approximated as 2. Values of $\mathcal{S}_k$ for the main paramagnetic species are summarized in Table II.

To provide insights into the mechanism of interaction between the magnetic field and the flame, the total force acting on the mixture, $\mathbf{f}_{KB^2} = \Sigma_{k=1}^{N}\mathbf{f}_k$, is decomposed using the Helmholtz decomposition[44] as

$$\mathbf{f}_{KB^2} = \mathbf{f}_{KB^2}^{irr} + \mathbf{f}_{KB^2}^{rot}, \tag{3}$$

where $\nabla \times \mathbf{f}_{KB^2}^{irr} = \mathbf{0}$ and $\nabla \cdot \mathbf{f}_{KB^2}^{rot} = 0$. The irrotational part of the magnetic force, $\mathbf{f}_{KB^2}^{irr}$, can be expressed as the gradient of a scalar potential ϕ_B, such that $\mathbf{f}_{KB^2}^{irr} = \nabla\phi_B$. For the leading-order

TABLE II. Total quantum spin numbers of the paramagnetic species in their fundamental state.[42]

Species	O_2	O	H	OH	HO_2
$\mathcal{S}_k$	1	1	1/2	1/2	1/2

02 October 2026 08:40:23

© Author(s) 2026

approximation of the Kelvin force, Eq. (1), this decomposition allows the separation of the component of $\mathbf{f}_{KB^2}$ that directly contributes to the pressure field, i.e., the irrotational component of the force, from the component that drives rotational fluid motion.

To investigate the mechanisms of vorticity generation by magnetic forcing, the vorticity equation is considered. By isolating the source terms associated with pressure and the irrotational and rotational components of the magnetic force, the vorticity equation reads

$$\frac{D\boldsymbol{\omega}}{Dt} = \frac{1}{\rho^2}\nabla\rho \times \left(\nabla P - \mathbf{f}^{irr}_{KB^2}\right) + \nabla \times \left(\frac{\mathbf{f}^{rot}_{KB^2}}{\rho}\right) + \mathcal{S}_{\tau_{ij}} + \mathcal{S}_{\omega}, \quad (4)$$

where $\boldsymbol{\omega}$ denotes the vorticity, P the pressure, t the time, $\mathcal{S}_{\tau_{ij}}$ represents the terms associated with the viscous stress tensor, and $\mathcal{S}_{\omega}$ represents the terms associated with dilatation (vortex stretching and tilting vanish in a two-dimensional configuration). In Eq. (4), the source term related to the rotational part of the magnetic force can be further decomposed as

$$\nabla \times \left(\frac{\mathbf{f}^{rot}_{KB^2}}{\rho}\right) = \frac{1}{\rho}\nabla \times \mathbf{f}^{rot}_{KB^2} - \frac{1}{\rho^2}\nabla\rho \times \mathbf{f}^{rot}_{KB^2}. \quad (5)$$

This decomposition is used in this work to separate the contribution arising from the misalignment between the density gradient and the rotational force from the direct contribution associated with the rotational content of $\mathbf{f}^{rot}_{KB^2}$.

In order to analyze the spatial distribution of the various quantities of interest across the flame front, the progress variable C_{H_2} is used,[46] defined from the mass fraction of hydrogen, Y_{H_2}, as

$$C_{H_2} = 1 - Y_{H_2}/Y_{H_{2,u}}, \quad (6)$$

where $Y_{H_{2,u}}$ is the hydrogen mass fraction in the unburnt mixture.

III. RESULTS AND DISCUSSION

The global response of the flame to the different magnetic fields is investigated first. Figure 3 shows the three main flame dynamics quantities, i.e., non-dimensional consumption speed, s_c/s_L, non-dimensional flame surface, A_f/A_0, and stretch factor, I_0 (usual notation applies), for all magnetic field configurations and both reactant conditions. In case 1, both the consumption speed and the flame surface decrease monotonically with increasing magnetic field strength, while I_0 remains approximately constant. This suggests that magnetic fields can affect the morphology of the flame by acting on the flame area. However, the local flame structure and chemistry are not significantly affected by the magnetic field, consistent with observations reported in Refs. 18 and 19. Conversely, in case 2, no clear trend is observed across all magnetic field configurations, suggesting that the magnetic field does not affect the flame dynamics in this high-pressure condition.

The absence of an effect of the magnetic field on the local structure and reactivity of the flame is further supported by Fig. 4, which shows the logarithmic joint probability density function of the reduced reaction rate as a function of the progress variable C_{H_2} for case 1 and magnetic field configurations (a) and (e). No significant changes in the distribution of the reaction rate across the reaction zone ($0.5 < C_{H_2} < 1.0$) are observed between the two magnetic field configurations, with the conditional averages remaining closely aligned across the entire range of C_{H_2}. Similar results are also found for case 2 (not shown here). This confirms that the reaction rate distribution across the flame front is unaffected by the magnetic field for all investigated cases.

An interesting metric for the evaluation of the local flame behavior is the size of the small-scale cellular structures that develop on the flame front. Figure 5 shows the probability density functions of the reduced radius of the small-scale flame cellular structures for all investigated cases. The distributions are nearly identical across all configurations of the magnetic field for both reactant conditions. In case 1, configuration (e) of the magnetic field exhibits a slightly higher peak in the probability density function. However, the inset box plots in Fig. 5 show substantially equal mean and median values across all configurations, indicating that this deviation remains marginal and that the overall small-scale flame geometry is not significantly altered by the magnetic field. The standard deviation of the reduced radius also appears similar across the various configurations, with no clear trends of variation with increasing strength of the magnetic field. Together with Fig. 4, these results indicate that the magnetic fields investigated here do not alter the local structure of the flame, its reactivity, and its

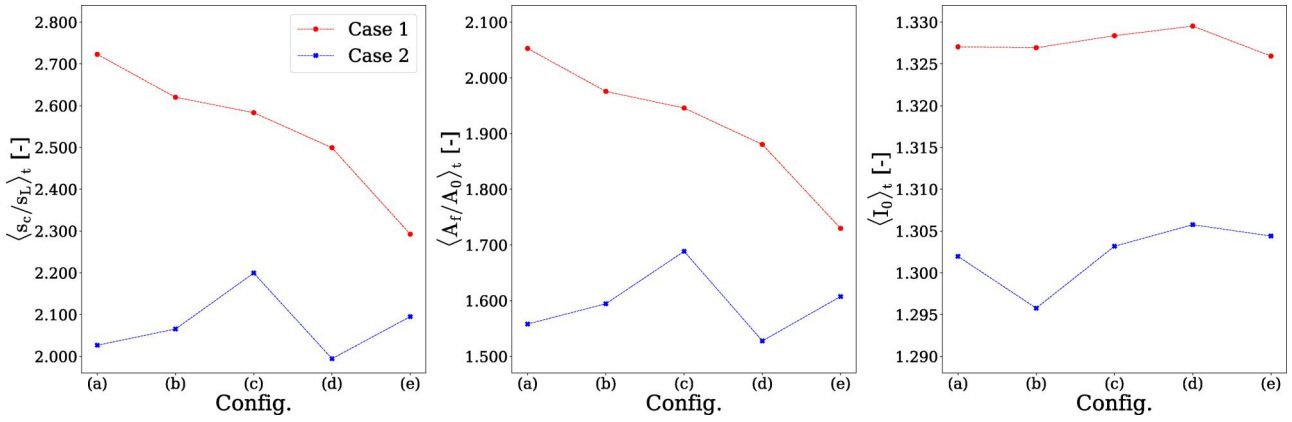


FIG. 3. Time-averaged non-dimensional flame consumption speed (left), flame surface (middle), and stretch factor (right) for magnetic field configurations (a)–(e). The various quantities are computed as in Ref. 45 and averaged over 200 flame times for case 1 and over 300 flame times for case 2.

02 October 2026 08:40:23

© Author(s) 2026

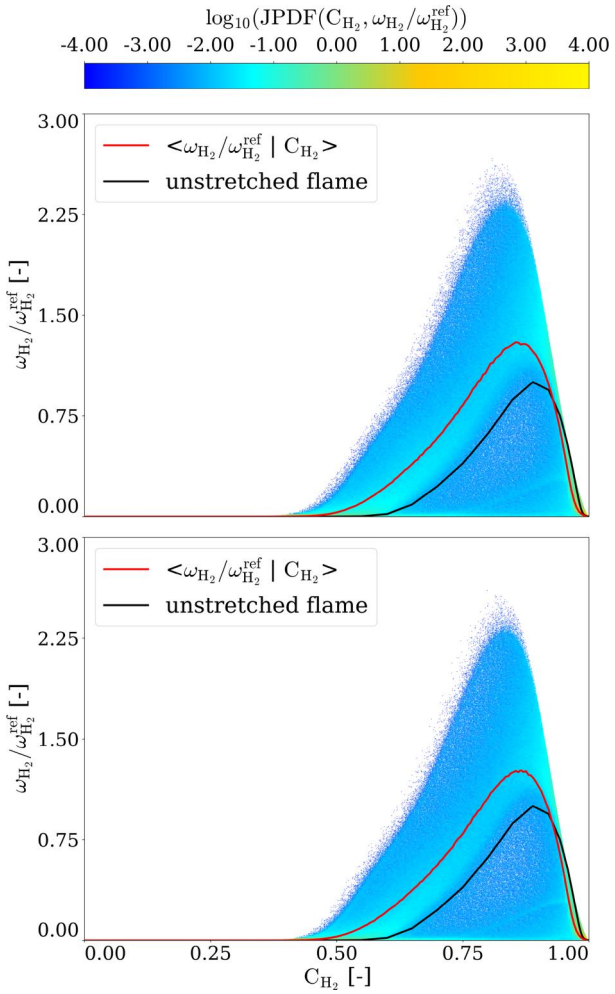


FIG. 4. Logarithmic joint probability density function of the reduced reaction rate $\omega_{H_2}/\omega^{ref}_{H_2}$ against the progress variable C_{H_2}, for case 1; magnetic field configuration (a) on the top and (e) on the bottom. The red and black lines represent the average of $\omega_{H_2}/\omega^{ref}_{H_2}$ conditioned on C_{H_2} and the unstretched (one-dimensional) profile of $\omega_{H_2}/\omega^{ref}_{H_2}$, respectively. The scaling is performed using the minimum reaction rate from the corresponding one-dimensional simulation.

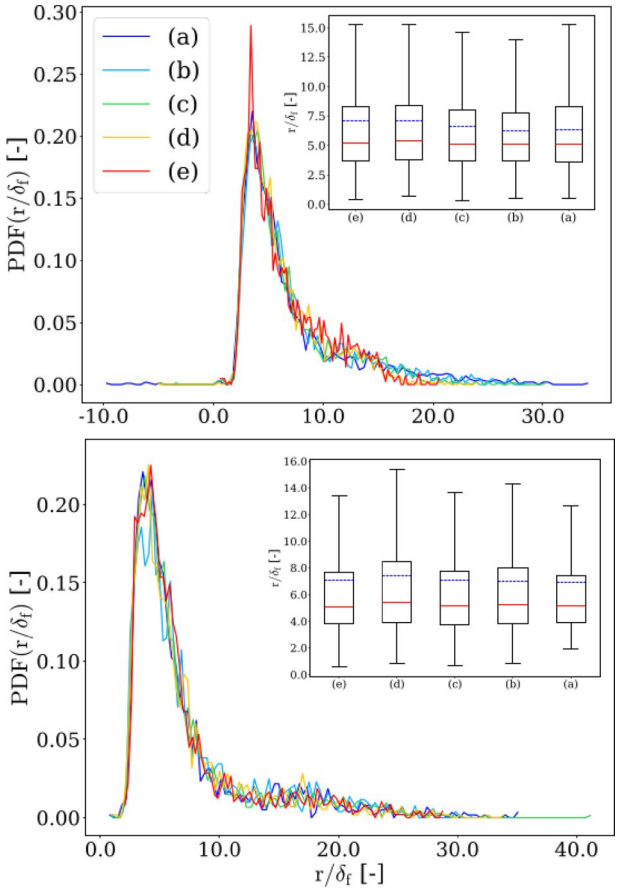


FIG. 5. Probability density function of the reduced radius of the small-scale flame cellular structures for magnetic field configurations (a)–(e), in case 1 (top) and case 2 (bottom). For each case, an inset box plot of the same quantity is shown, with the mean indicated by a dashed blue line and the median by a solid red line.

small-scale structures. Therefore, in the cases investigated in the present study, the thermodiffusive instability appears not to be affected by the presence of a magnetic field. Therefore, the reduction in s_c/s_L observed in Fig. 3 for the case with reactants at atmospheric conditions is of purely fluid mechanics origin, as also suggested by the decrease in flame area. This indicates that the magnetic field primarily affects the hydrodynamic (Darrieus–Landau) instability. Effects on thermodiffusive instability may require higher gradients of the magnetic field, which should be investigated in future work.

To investigate this hydrodynamic effect, Fig. 6 shows the vorticity distribution as a function of the progress variable C_{H_2} for case 1 and the two extreme configurations of no magnetic field and magnetic field with the strongest gradient, i.e., configurations (a) and (e). Results show that the distribution of vorticity across the flame changes significantly when magnetic forces are introduced in the domain. The conditional average remains centered around zero, indicating no preferential rotation in the flow field on both sides of the flame front. However, in the presence of a magnetic field, the distribution of vorticity in the reaction zone ($0.5 < C_{H_2} < 1.0$) develops two distinct peaks in probability (shown by the cyan regions in Fig. 6) at positive and negative values of vorticity. This means that although the extreme vorticity values are not significantly altered by the magnetic field, there are regions in the flame where higher magnitudes of vorticity are more probable. Inspection of the results from all the investigated cases indicates that the distance between these two peaks (i.e., stronger vorticity, both positive and negative) increases with increasing strength of the applied magnetic field gradient. The effect of the magnetic field on the vorticity is further investigated through Fig. 7, which shows the conditional average (with respect to C_{H_2}) of the magnitude of the vorticity for case 1 and all the investigated magnetic field configurations. Results indicate that the average vorticity magnitude across the flame increases with increasing strength of the applied magnetic field gradient, especially for magnetic field configurations (c)–(e); it is also worth noting that for $C_{H_2} > 0.95$, the average

02 October 2026 08:40:23

© Author(s) 2026

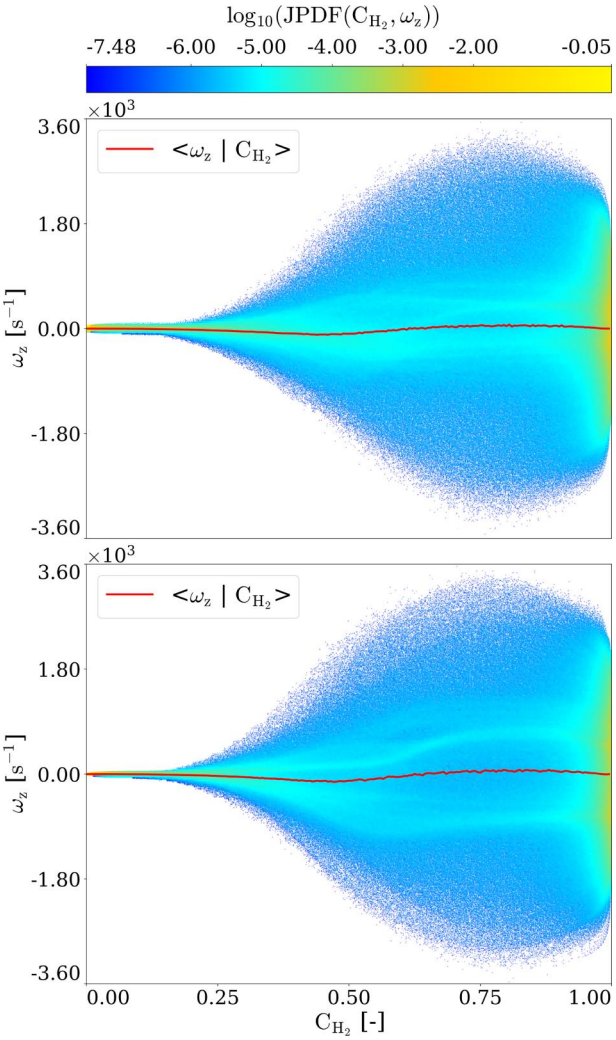


FIG. 6. Logarithmic joint probability density functions of the z-component of the vorticity field, ω_z, against the progress variable, C_{H_2}, for case 1; magnetic field configuration (a) on the top and (e) on the bottom. The red lines represent the conditional average of ω_z with respect to C_{H_2}.

vorticity magnitude consistently increases with increasing magnetic field gradient, indicating an increase in vorticity in the regions downstream of the flame front. This suggests that the magnetic field generates vortical structures that interact with the flame front. In the present configuration, these structures act to smooth the flame surface, resulting in a reduced flame surface area and consequently a reduced consumption speed, consistent with Fig. 3. Note that in case 2, no significant variation in the vorticity distribution is observed across all configurations (not shown here), consistent with the absence of clear effects of the magnetic field on the flame behavior.

The effect of magnetic forces on the flow field is further investigated by means of Fig. 8, which shows the vorticity field at a selected time instant for the two conditions analyzed in Fig. 6. At the same simulated time, the configuration with a magnetic field exhibits higher

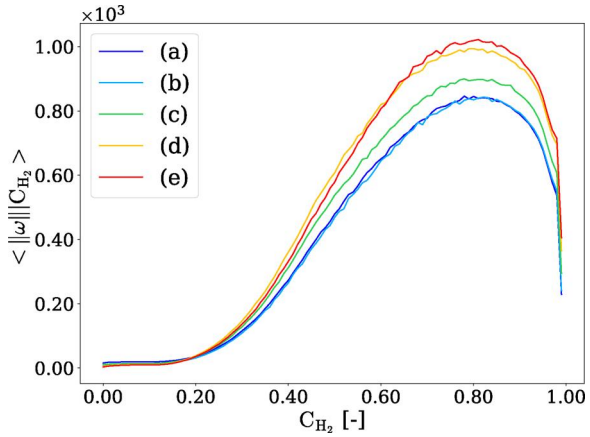


FIG. 7. Conditional average of the magnitude of the vorticity field, $\|\omega\|$, with respect to the progress variable, C_{H_2}, for case 1 and magnetic field configurations (a)–(e).

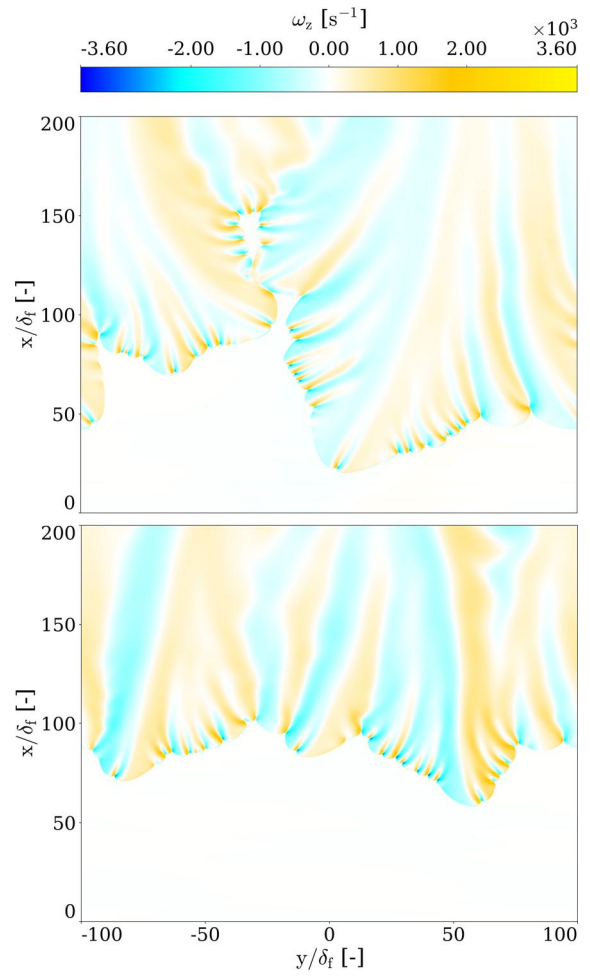


FIG. 8. Instantaneous z-component of the vorticity field, ω_z, at $t \approx 200\,\tau_f$, for case 1; magnetic field configuration (a) on the top and (e) on the bottom.

02 October 2026 08:40:23

© Author(s) 2026

vorticity magnitudes downstream of the flame front compared to the case without a magnetic field. In addition, it is evident that the size of the flame fingers, i.e., the Darrieus–Landau instability, is significantly reduced by the presence of a magnetic field, resulting in a smaller surface area. This structure of the vorticity field and its variation when a magnetic field is applied smooth the flame finger structures, driving the decrease in the flame surface observed in the time-averaged statistics.

To gain more insight into the mechanism leading to the hydrodynamic effects of a magnetic field, the forces acting on the flow are discussed next. Figure 9 shows the x- and y-components of the pressure gradient and the Kelvin force for the atmospheric pressure condition (case 1) and the magnetic field configuration with the strongest gradient. Magnetic force components resulting from the decomposition of the Kelvin force into irrotational and rotational parts are also shown. For the irrotational component of the magnetic force, the difference between the pressure gradient and this component is presented. Results demonstrate that the x-component of the pressure gradient, $(\nabla \mathrm{P})_x$, is significantly affected by the presence of the magnetic field. Close to the inlet, the values of the pressure gradient tend to balance the Kelvin force, $\mathrm{f}_{\mathrm{KB}^2,x}$. Both these forces exhibit negative values consistent with the orientation of $\nabla(\mathrm{B}^2)$ toward the inlet. As the flame front is approached, larger differences between the gradient of pressure and the Kelvin force are observed. The pressure gradient exhibits larger magnitudes along the flame front, while the magnetic force transitions toward the values found on the product side of the flame without peaks on the flame front. Past the flame front, in the product region, both recover a similar spatial distribution, with magnitudes of the magnetic force that tend to zero. This attenuation of the magnetic forces moving from the reactant to the product side of the flame is primarily driven by the inverse dependence of the magnetic susceptibility on temperature. This is combined with the reduction of the mass fraction of oxygen in the product region, which is the species with the highest susceptibility and the one that contributes mostly to the overall magnetic force.

Analysis of the irrotational and rotational components of the magnetic force shows that the difference $(\nabla \mathrm{P})_x - \mathrm{f}^{\mathrm{irr}}_{\mathrm{KB}^2,x}$ is small in the reactant region and cancels on either side of the flame fingers in the vicinity of the flame front, with the exception of regions that show high flame curvature (see Fig. 9, top). The rotational component of the magnetic force, $\mathrm{f}^{\mathrm{rot}}_{\mathrm{KB}^2,x}$, pushes the flame fingers in the positive x-direction while pulling the troughs between adjacent flame fingers toward the negative x-direction, thereby contributing to the flattening of the flame front and the generation of vortical structures discussed previously. In the region immediately downstream of the flame fingers, the rotational term constitutes the sole effective force contribution, as $(\nabla \mathrm{P})_x$ and $\mathrm{f}^{\mathrm{irr}}_{\mathrm{KB}^2,x}$ tend to cancel each other, while on the flame front itself the pressure gradient remains the dominant term. Note that across the flame front, the flame is characterized by a gradient in density, which leads to an acceleration of the flow.

The contribution of forces is further analyzed by considering the y-component of the forces (Fig. 9, bottom). $(\nabla \mathrm{P})_y$ exhibits an antisymmetric pattern along the flame front, such that the gradient of pressure, driven by the increase in temperature from reactants to products, tends to point toward the reactants. The y-component of $\mathbf{f}_{\mathrm{KB}^2}$ is negligible, as the magnetic field gradient is predominantly oriented along x, although the symmetry of the magnetic forces with respect to the x axis ($y = 0$) remains visible in the force field. The

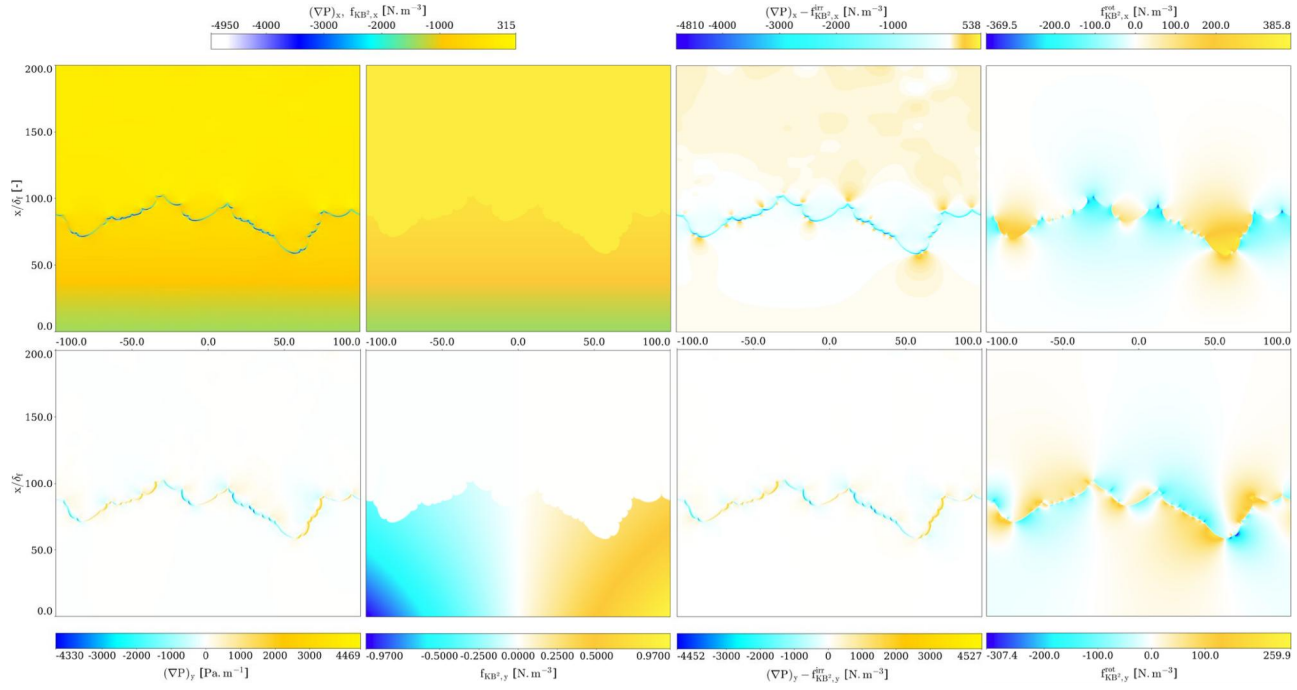


FIG. 9. Instantaneous fields at $t \approx 200\,\tau_f$ for case 1 and magnetic field configuration (e); x-component (top row) and y-component (bottom row) of (from left to right) the pressure gradient $\nabla \mathrm{P}$, the total Kelvin force density $\mathbf{f}_{\mathrm{KB}^2}$, the difference $\nabla \mathrm{P} - \mathbf{f}^{\mathrm{irr}}_{\mathrm{KB}^2}$, and the rotational component $\mathbf{f}^{\mathrm{rot}}_{\mathrm{KB}^2}$.

02 October 2026 08:40:23

© Author(s) 2026

difference $(\nabla P)_y - f^{irr}_{KB^2,y}$ is completely dominated by the pressure gradient, and $f^{rot}_{KB^2,y}$ displays a pattern consistent with a closing motion of the flame fingers, further supporting the action of the rotational forces toward reducing the flame area. The action of the rotational force on the flame front is further elucidated by means of Fig. 10, which shows the magnitude of the rotational component of the magnetic force, with the corresponding force field lines overlaid. It is interesting to note that the rotational forces show a "circular" pattern along the sides of the flame fingers, with the direction of rotation that promotes the flattening of the flame front. Note that in case 2 (not shown here), ∇P is orders of magnitude larger than the magnetic force for all magnetic field configurations, which further supports the absence of significant effects of the magnetic field on the flame dynamics.

Other decompositions of the magnetic force proposed in the literature can provide further insights into the conditions needed to establish rotational forces. A common approach to decompose the magnetic force separates the Kelvin force density of Eq. (1) into a gradient of the so-called magnetically induced pressure and a magnetic Korteweg–Helmholtz term.[24,47] The former component is irrotational and tends to be balanced by the pressure gradient,[47] as also observed for the flame discussed in this study (e.g., see the reactant region in Fig. 9). The Korteweg–Helmholtz term, equal to $-B^2\nabla\chi/(2\mu_0)$, is proportional to the gradient of mixture susceptibility and contains both irrotational and rotational contributions. This implies that a gradient in the mixture susceptibility is a necessary condition for the existence of rotational components of the magnetic force. Taking the curl of the Korteweg–Helmholtz force shows that this term acts as a source of vorticity when the gradient in mixture susceptibility is not aligned with the gradient of the square of the magnetic field.[48] The relation between the gradient in mixture susceptibility and the rotational component of the magnetic force is further analyzed in Fig. 11, which shows the joint probability distributions of the curl of the Korteweg–Helmholtz force with respect to the progress variable and the correlation of this quantity with the curl of the rotational component of the magnetic force for case 1 and the magnetic field configuration (e). Results indicate that the direct generation of vorticity from the misalignment between the gradient of susceptibility and the gradient of the square of the magnetic field is confined within the reaction zone, where the variations in temperature and composition of the mixture lead to gradients of susceptibility. In addition, results indicate that the curl of the rotational force obtained from the Helmholtz decomposition is perfectly correlated with the curl of the Korteweg–Helmholtz force, further supporting the cause–effect relation between gradients of mixture susceptibility and generation of rotational forces. It is worth noting that, as illustrated in Fig. 9, rotational forces also

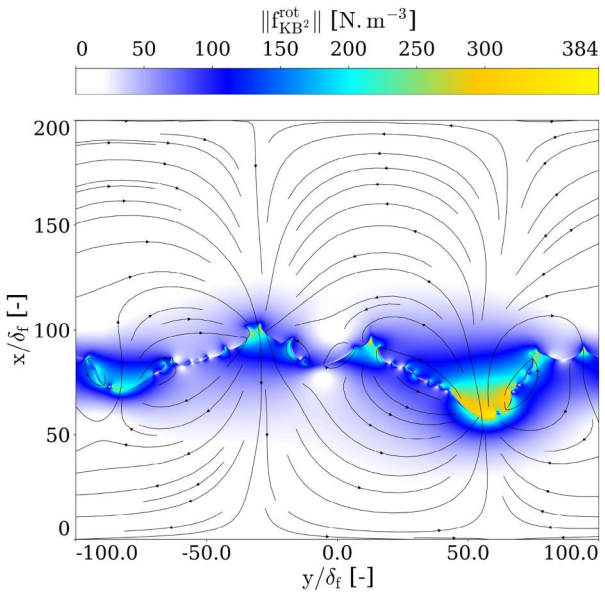


FIG. 10. Instantaneous magnitude of the rotational component of the magnetic force, $\|f^{rot}_{KB^2}\|$, at $t \approx 200\ \tau_f$, for case 1, magnetic field configuration (e). The black lines correspond to the force field lines, i.e., lines that are locally tangent to the rotational force vectors.

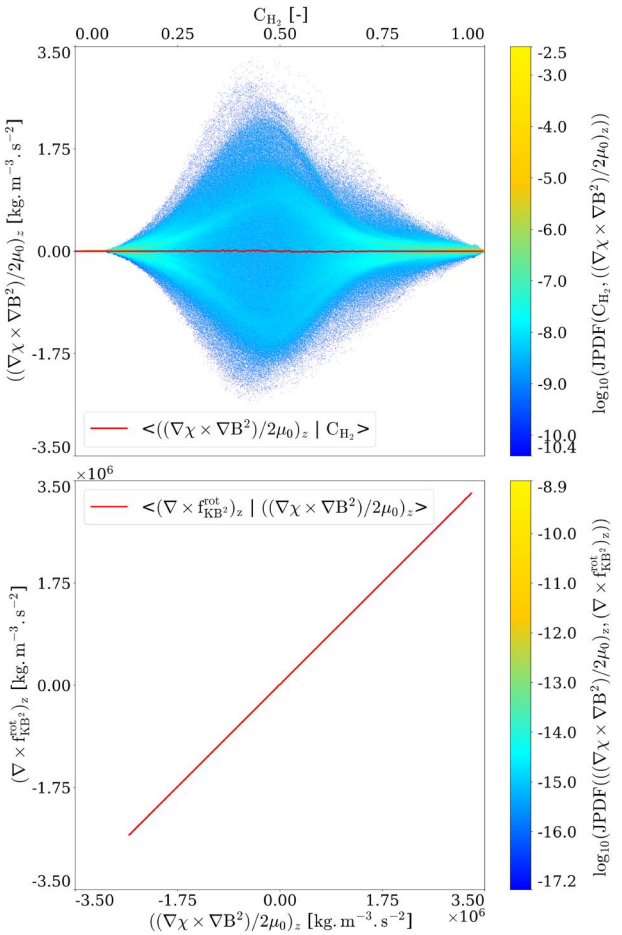


FIG. 11. Logarithmic joint probability density functions of the z-component of the curl of the Korteweg–Helmholtz force against the progress variable, C_{H_2} (top), and the curl of the rotational part of the magnetic force obtained from the decomposition in Eq. (3) against the curl of the Korteweg–Helmholtz force, for case 1 and magnetic field configuration (e). The red lines represent the conditional average of the considered quantities.

02 October 2026 08:40:23

© Author(s) 2026

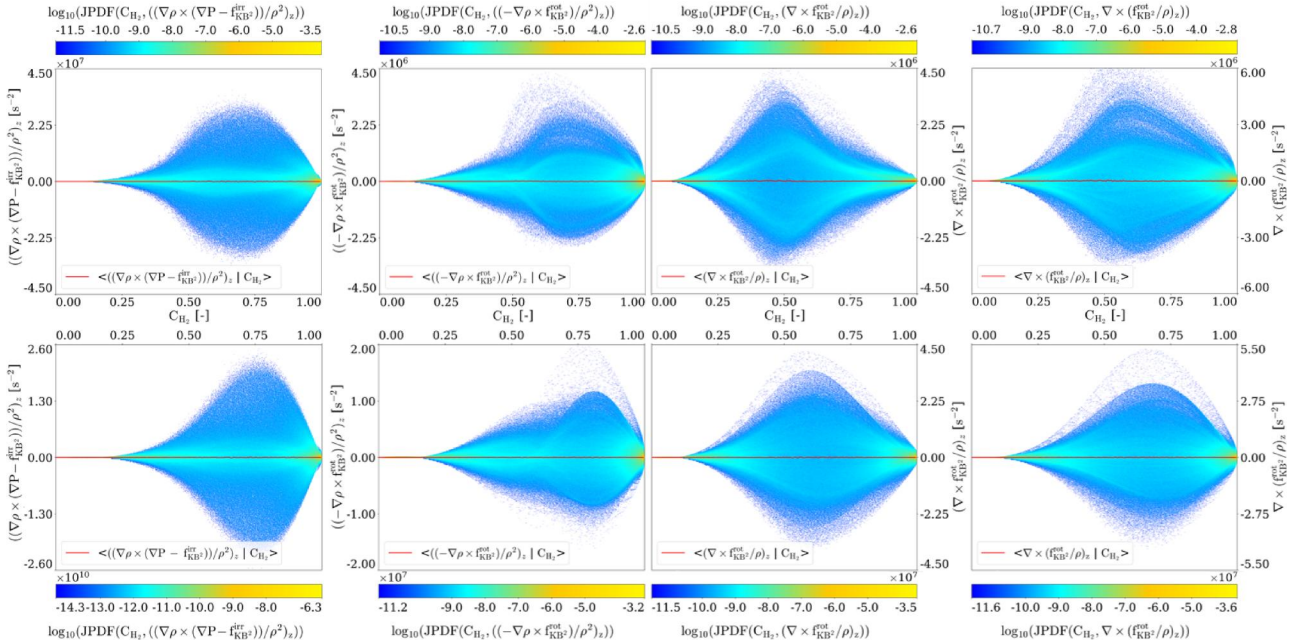


FIG. 12. Logarithmic joint probability density functions, with respect to the progress variable, C_{H_2}, of the various contributions to the *z*-component of the vorticity for case 1 (top) and case 2 (bottom) and the magnetic field configuration (e). From left to right, the figure shows the contribution due to the difference between the pressure gradient and irrotational force, $\nabla\rho \times (\nabla P - \mathbf{f}^{irr}_{KB^2})/\rho^2$; the two contributions due to the rotational force, $-\nabla\rho \times \mathbf{f}^{rot}_{KB^2}/\rho^2$ and $\nabla \times \mathbf{f}^{rot}_{KB^2}/\rho$; and the total contribution of the rotational force (sum of the two previous terms) $\nabla \times (\mathbf{f}^{rot}_{KB^2}/\rho)$, against the progress variable C_{H_2}. The red lines represent the conditional average of the considered quantities.

appear in regions without significant gradients in mixture susceptibility (the same force contribution would be obtained by isolating the rotational component of the Korteweg–Helmholtz force). This is a consequence of the Helmholtz decomposition. In these regions, the contribution of rotational forces to the vorticity generation is negligible.

To investigate the mechanisms leading to the changes in vorticity under a magnetic field, Fig. 12 shows the joint probability distributions with respect to the progress variable, C_{H_2}, of the source terms in the vorticity equation associated with the magnetic force and the pressure gradient [see Eqs. (4) and (5)], for case 1 (top row) and case 2 (bottom row) under the magnetic field configuration (e). The results demonstrate that, in both cases, the sources of vorticity peak in the reaction zone and that the term related to the pressure gradient is the dominant term in vorticity generation. Analysis of the term given by the difference between the pressure gradient and the irrotational component of the magnetic force (first column in Fig. 12) indicates that this contribution is only marginally affected by the magnetic field (other magnetic fields, not shown here, show a very similar distribution). This is consistent with the fact that the irrotational component of the magnetic force tends to be balanced by variations in the pressure gradient. Further insight into the generation of vorticity by magnetic forces is provided by the terms associated with the rotational component of the magnetic force (second and third columns in Fig. 12). The term in the second column is mainly driven by the density gradient, while the term in the third column represents the direct contribution of the rotational part of the magnetic force to the vorticity generation. In case 1, these two terms span similar ranges of values,

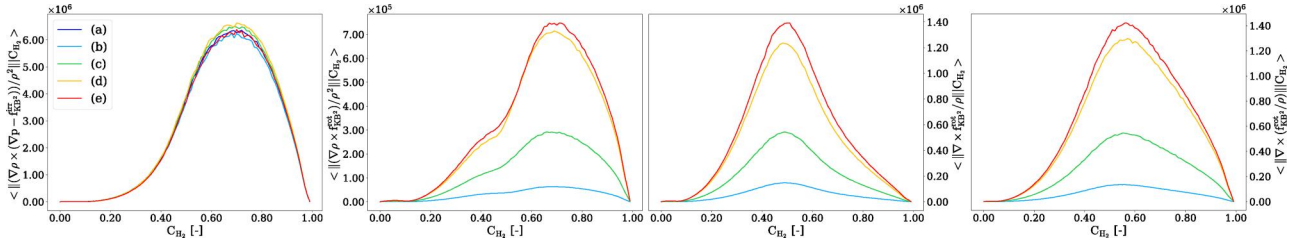


FIG. 13. Conditional averages, with respect to the progress variable, C_{H_2}, of the magnitude of the vorticity source terms for case 1 and magnetic field configurations (a)–(e). From left to right, the figure shows the contribution due to the difference between the pressure gradient and irrotational force, $\nabla\rho \times (\nabla P - \mathbf{f}^{irr}_{KB^2})/\rho^2$, with only the pressure gradient contribution for configuration (a); the two contributions due to the rotational force, $-\nabla\rho \times \mathbf{f}^{rot}_{KB^2}/\rho^2$ and $\nabla \times \mathbf{f}^{rot}_{KB^2}/\rho$; and the total contribution of the rotational force (sum of the two previous terms) $\nabla \times (\mathbf{f}^{rot}_{KB^2}/\rho)$, against the progress variable C_{H_2}.

02 October 2026 08:40:23

© Author(s) 2026

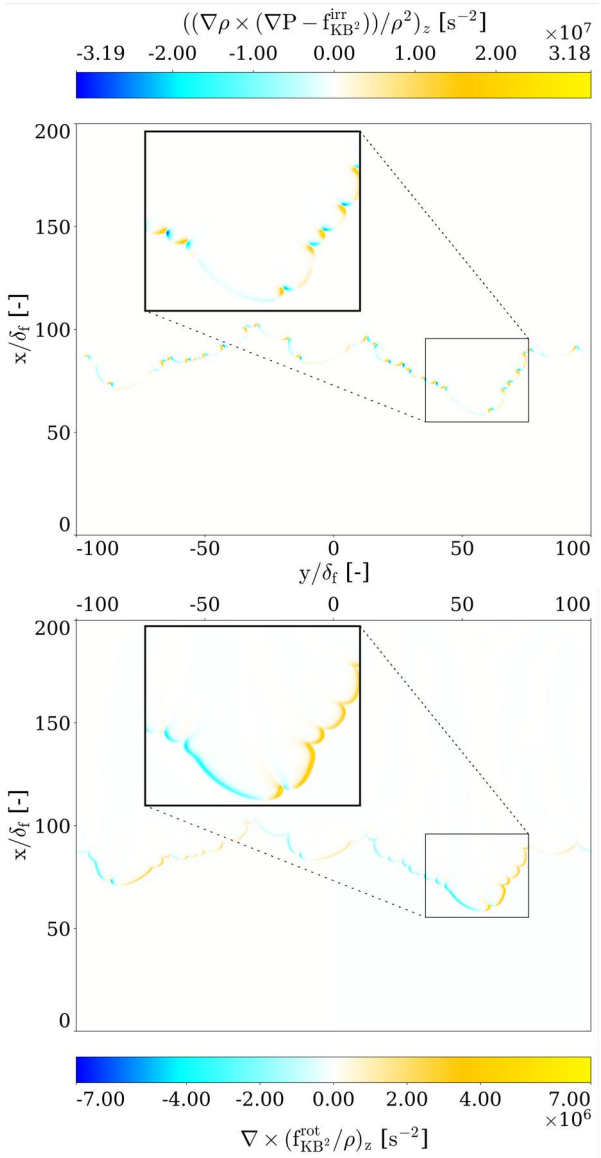


FIG. 14. Instantaneous z-component of the source terms of the vorticity field: the term related to the difference between the pressure gradient and irrotational force, i.e., the contribution from all irrotational forces (including pressure forces), $\nabla\rho \times (\nabla P - \mathbf{f}^{irr}_{KB^2})/\rho^2$ (top), and the contribution of the rotational component of the magnetic force $\nabla \times (\mathbf{f}^{rot}_{KB^2}/\rho)$ (bottom), at $t \approx 200\,\tau_f$, for case 1 and magnetic field configuration (e). The insets marked by the black frames provide a zoomed-in view of a flame finger.

and, when combined (last column in Fig. 12), their magnitude becomes comparable to that of the pressure and irrotational term, leading to the changes in vorticity observed in Fig. 6. The variation of the sources of vorticity with increasing magnetic field gradient is demonstrated in Fig. 13, which shows the conditional average (with respect to the progress variable) of the vorticity sources. First, it is interesting to note that the vorticity source associated with the term given by the combination of the pressure gradient and the irrotational part of the magnetic force is similar for all the investigated magnetic fields and does not show any significant changes compared to the case without magnetic fields. This provides evidence that as the magnetic field gradient increases, the pressure gradient also tends to increase to balance the irrotational part of the magnetic force. Instead, all source terms related to the rotational part of the force progressively increase with increasing magnetic field gradient, with a magnitude increasingly close to the values of the source associated with the pressure and irrotational component of the magnetic force. This causes the reduction in the flame area to increase with the magnetic field gradient. Conversely, in case 2, the source term related to the pressure gradient is three orders of magnitude higher than the contributions given by the magnetic forces (see Fig. 12, bottom), which are therefore too weak to cause any significant changes in vorticity.

The mechanism of interaction between magnetic forces and the flame front is further investigated through Fig. 14, which shows the spatial distribution of vorticity sources, separated into terms related to irrotational and rotational forces, at a selected time instant for case 1 and magnetic field configuration (e). The vorticity sources are confined within the reaction layer. The sources of vorticity due to all irrotational forces (including pressure forces, i.e., $\nabla P - \mathbf{f}^{irr}_{KB^2}$) peak at the tip of the fingers and small-scale cellular structures and alternate between positive and negative values around these peaks. Conversely, the source term related to the rotational component of the magnetic force is more uniformly distributed along the flame front, with opposite values on the two sides of the flame fingers. More specifically, the contribution of the rotational force to the vorticity sources is positive or negative depending on the orientation of the gradient of susceptibility (pointing toward the reactants) with respect to the gradient of the magnetic field magnitude. Comparison with Fig. 8 demonstrates that the sources related to rotational forces are responsible for the increase in vorticity (either more positive or more negative values) observed on either side of the flame fingers in the product region of the flame, compared to the case without magnetic fields. In addition, comparison between Figs. 14 and 10 clearly shows that the direction of the rotational force field is well correlated with the sources of vorticity on the flame front, further highlighting the link between these forces, the generation of vorticity, and the consequent effect on the flame dynamics. This provides further evidence of the mechanism of interaction between the magnetic forces, in particular their rotational component, and the flame front, which in the investigated configuration tends to reduce the hydrodynamic instabilities. It is worth noting that the present investigation was conducted in a two-dimensional domain, where the absence of vortex stretching may lead to more persistent vortical structures than in a three-dimensional configuration. Although this does not affect the mechanism of interaction between the magnetic forces and the flame front, a three-dimensional configuration may require different magnetic fields to achieve the same effects. Extension of the present investigation to three-dimensional domains, including more complex shapes of the magnetic field and different equivalence ratios, as well as the development of experiments to corroborate the present findings, is part of future research. It should also be noted that, since the dominant magnetic response originates from oxygen rather than the fuel, the use of magnetic forces to control the flame dynamics is not inherently restricted to hydrogen–air combustion. The identified mechanism, namely, the generation of

02 October 2026 08:40:23

© Author(s) 2026

a rotational magnetic force from susceptibility gradients and the effect on vorticity, is expected to remain qualitatively valid also in flames generated with different fuels, even though the field strength needed to produce an observable effect will depend on the properties of the fuel considered and the resulting characteristics of the flame front. Future research should focus on quantifying these effects with the perspectives provided by the present work.

IV. CONCLUSIONS

The effect of magnetic forces on the dynamics of premixed laminar hydrogen–air flames has been investigated using direct numerical simulations for different conditions of the reactants and various strengths of the magnetic forces. Results show that at atmospheric pressure, magnetic forces affect the flame speed through changes in the flame area, whereas at high pressure, effects are negligible over the simulated flame time. A gradient in the magnetic field magnitude oriented opposite to the velocity of the incoming reactants leads to a decrease in the flame consumption speed, an effect that increases with increasing magnetic field gradients. For all investigated magnetic field configurations, the effect of magnetic forces on the local flame structure is negligible at both atmospheric and high pressures, as demonstrated by the absence of significant changes in the stretch factor and by statistics of the hydrogen reaction rate. Investigation of the small-scale cellular structures developed along the flame front also shows that magnetic fields do not alter their statistics, suggesting that the thermodiffusive instability remains unchanged for all magnetic fields investigated here. Investigation of the forces and their spatial distribution demonstrates the role of the rotational component of the magnetic force on the reduction in the flame area observed at atmospheric conditions. Analysis of the vorticity source terms associated with the various forces establishes a relation between the rotational component of the magnetic force and the increase in vorticity observed on the flame front and on the product side of the flame. This change in vorticity results in an alteration of the flame dynamics such that the fingerlike structures formed by Darrieus–Landau instabilities tend to reduce with increasing gradient of the magnetic field. The role of gradients in susceptibility in the establishment of rotational forces and vorticity source terms is also highlighted, providing further insight into the origin of the effect of magnetic forces on the flame behavior. Ultimately, the results of this work indicate that magnetic forces have the potential to modify the flame surface and stability, suggesting a possible avenue for the mitigation of intrinsic flame instabilities and the active control of the flame behavior.

ACKNOWLEDGMENTS

T.L. and A.G. acknowledge financial support from UKRI EPSRC Grant Ref. No. EP/Y031423/1, which is part of the ICHAruS project, funded by the European Union under the Horizon Europe Program, Grant No. 101120321. We also acknowledge the computational resources and support provided by the Imperial College Research Computing Service (doi.org/10.14469/hpc/2232).

AUTHOR DECLARATIONS

Conflict of Interest

The authors have no conflicts to disclose.

Author Contributions

Tristan Lapaire: Conceptualization (equal); Data curation (lead); Formal analysis (lead); Investigation (lead); Methodology (lead); Software (lead); Validation (lead); Visualization (lead); Writing – original draft (lead); Writing – review & editing (equal). **Sofiane Al Kassar:** Methodology (supporting); Software (supporting); Writing – review & editing (supporting). **Antonio Attili:** Formal analysis (supporting); Methodology (supporting); Resources (equal); Software (supporting); Writing – review & editing (supporting). **Andrea Giusti:** Conceptualization (equal); Formal analysis (supporting); Funding acquisition (lead); Investigation (supporting); Methodology (supporting); Resources (equal); Supervision (lead); Writing – review & editing (equal).

DATA AVAILABILITY

The data that support the findings of this study are available from the corresponding author upon reasonable request.

REFERENCES

[1]M. Fontecave, S. Candel, and T. Poinsot, "Hydrogen today and tomorrow," Technical Report No. HAL-04678172 (Académie des Sciences, 2024).
[2]S. Taamallah, K. Vogiatzaki, F. Alzahrani, E. Mokheimer, M. Habib, and A. Ghoniem, "Fuel flexibility, stability and emissions in premixed hydrogen-rich gas turbine combustion: Technology, fundamentals, and numerical simulations," Appl. Energy **154**, 1020–1047 (2015).
[3]G. Darrieus, "Propagation d'un front de flamme," La Technique Moderne **30** (1938).
[4]C. K. Law, *Combustion Physics* (Cambridge University Press, 2010).
[5]M. Matalon, "Intrinsic flame instabilities in premixed and nonpremixed combustion," Annu. Rev. Fluid Mech. **39**, 163–191 (2007).
[6]M. Matalon, "The Darrieus–Landau instability of premixed flames," Fluid Dyn. Res. **50**, 051412 (2018).
[7]C. Altantzis, C. Frouzakis, A. Tomboulides, M. Matalon, and K. Boulouchos, "Hydrodynamic and thermodiffusive instability effects on the evolution of laminar planar lean premixed hydrogen flames," J. Fluid Mech. **700**, 329–361 (2012).
[8]L. Berger, K. Kleinheinz, A. Attili, and H. Pitsch, "Characteristic patterns of thermodiffusively unstable premixed lean hydrogen flames," Proc. Combust. Inst. **37**, 1879–1886 (2019).
[9]L. Berger, A. Attili, and H. Pitsch, "Intrinsic instabilities in premixed hydrogen flames: Parametric variation of pressure, equivalence ratio, and temperature. Part 1—Dispersion relations in the linear regime," Combust. Flame **240**, 111935 (2022).
[10]L. Berger, A. Attili, and H. Pitsch, "Intrinsic instabilities in premixed hydrogen flames: Parametric variation of pressure, equivalence ratio, and temperature. Part 2—Non-linear regime and flame speed enhancement," Combust. Flame **240**, 111936 (2022).
[11]A. Aniello, D. Laera, S. Marragou, H. Magnes, L. Selle, T. Schuller, and T. Poinsot, "Experimental and numerical investigation of two flame stabilization regimes observed in a dual swirl H_2-air coaxial injector," Combust. Flame **249**, 112595 (2023).
[12]W. Liu and W. Jones, "Differential diffusion effects in a lean-premixed bluff-body stabilized hydrogen flame," Combust. Flame **284**, 114682 (2026).
[13]Y. Liao, Y. Choi, P. Liu, K. T. Kim, and Y. Guan, "Active control of thermoacoustic instability in a lean-premixed hydrogen-enriched combustor via open-loop acoustic forcing," Combust. Flame **277**, 114175 (2025).
[14]J.-B. Perrin-Terrin, N. Vaysse, D. Durox, R. Vicquelin, S. Candel, C. O. Laux, and A. Renaud, "Plasma-assisted combustion of hydrogen swirling flames: Extension of lean blowout limit and NO_x emissions," Proc. Combust. Inst. **40**, 105546 (2024).
[15]A. Ånestad, E. AEsøy, J. R. Dawson, and N. A. Worth, "Mitigating thermoacoustic instabilities in premixed hydrogen flames using axial staging," Proc. Combust. Inst. **40**, 105430 (2024).

02 October 2026 08:40:23

© Author(s) 2026

[16]M. Faraday, "LXIV. On the diamagnetic conditions of flame and gases," London, Edinburgh Dublin Philos. Mag. J. Sci. **31**, 401–421 (1847).
[17]E. Yamada, M. Shinoda, H. Yamashita, and K. Kitagawa, "Experimental and numerical analyses of magnetic effect on OH radical distribution in a hydrogen-oxygen diffusion flame," Combust. Flame **135**, 365–379 (2003).
[18]S. Kinoshita, T. Takagi, H. Kotera, and N. I. Wakayama, "Numerical simulation of diffusion flames with and without magnetic field," IEEE Trans. Appl. Supercond. **14**, 1685–1688 (2004).
[19]J. Hosseinpour and H. Mahdavy-Moghaddam, "Computational study of magnetic field effects on the nozzle of hydrogen micro flame," Combust. Flame **220**, 247–256 (2020).
[20]V. M. Natesh and I. Langella, "Influence of magnetic field on flame dynamics in hydrogen flames: A numerical study," Proc. Combust. Inst. **41**, 105892 (2025).
[21]N. I. Wakayama, "Behavior of gas flow under gradient magnetic fields," J. Appl. Phys. **69**, 2734–2736 (1991).
[22]N. I. Wakayama, "Magnetic acceleration and deceleration of O_2 gas streams injected into air," IEEE Trans. Magn. **31**, 897–901 (1995).
[23]E. Yamada, M. Shinoda, H. Yamashita, and K. Kitagawa, "Numerical analysis of a hydrogen-oxygen diffusion flame in vertical or horizontal gradient of magnetic field," Combust. Sci. Technol. **174**, 149–164 (2002).
[24]J. R. Melcher, *Continuum Electromechanics* (MIT Press, Cambridge, MA, 1981).
[25]Y. Mizutani, M. Fuchihata, and Y. Ohkura, "Pre-mixed laminar flames in a uniform magnetic field," Combust. Flame **125**, 1071–1073 (2001).
[26]M. Ortner and L. G. C. Bandeira, "Magpylib: A free Python package for magnetic field computation," SoftwareX **11**, 100466 (2020).
[27]S. Al Kassar, L. Berger, P. E. Lapenna, F. Creta, H. Pitsch, and A. Attili, "Efficient and accurate calculation of dispersion relations for intrinsically unstable premixed flames," Combust. Flame **269**, 113640 (2024).
[28]A. Tomboulides, J. Lee, and S. Orszag, "Numerical simulation of low Mach number reactive flows," J. Sci. Comput. **12**, 139–167 (1997).
[29]M. P. Burke, M. Chaos, Y. Ju, F. L. Dryer, and S. J. Klippenstein, "Comprehensive H_2/O_2 kinetic model for high-pressure combustion," Int. J. Chem. Kinet. **44**, 444–474 (2012).
[30]C. R. Wilke, "A viscosity equation for gas mixtures," J. Chem. Phys. **18**, 517–519 (1950).
[31]R. B. Bird, "Transport phenomena," Appl. Mech. Rev. **55**, R1–R4 (2002).
[32]A. Attili, F. Bisetti, M. E. Mueller, and H. Pitsch, "Effects of non-unity Lewis number of gas-phase species in turbulent nonpremixed sooting flames," Combust. Flame **166**, 192–202 (2016).
[33]F. A. Williams, *Combustion Theory*, 2nd ed. (CRC Press, 2018).
[34]J. O. Hirschfelder, C. F. Curtiss, and R. B. Bird, *The Molecular Theory of Gases and Liquids* (John Wiley & Sons, 1964).
[35]T. Zirwes and A. Kronenburg, "Assessment of approximate Soret diffusion models for hydrogen and ammonia combustion," Flow, Turbul. Combust. **115**, 1631 (2025).
[36]O. Desjardins, G. Blanquart, G. Balarac, and H. Pitsch, "High order conservative finite difference scheme for variable density low Mach number turbulent flows," J. Comput. Phys. **227**, 7125–7159 (2008).
[37]K. Niemietz, L. Berger, M. Huth, A. Attili, and H. Pitsch, "Direct numerical simulation of flame-wall interaction at gas turbine relevant conditions," Proc. Combust. Inst. **39**, 2209–2218 (2023).
[38]T. Poinsot and D. Veynante, *Theoretical and Numerical Combustion* (R. T. Edwards, Inc., 2005).
[39]X.-D. Liu, S. Osher, and T. Chan, "Weighted essentially non-oscillatory schemes," J. Comput. Phys. **115**, 200–212 (1994).
[40]A. C. Hindmarsh, P. N. Brown, K. E. Grant, S. L. Lee, R. Serban, D. E. Shumaker, and C. S. Woodward, "Sundials: Suite of nonlinear and differential/algebraic equation solvers," ACM Trans. Math. Software **31**, 363–396 (2005).
[41]P. Curie, *Propriétés Magnétiques Des Corps a Diverses Températures* (Gauthier-Villars et fils, 1895).
[42]G. M. Barrow, *Physical Chemistry*, 6th ed. (McGraw-Hill, 1996).
[43]G. Herzberg, *Atomic Spectra and Atomic Structure* (Dover Publications, 1944).
[44]G. K. Batchelor, *An Introduction to Fluid Dynamics* (Cambridge University Press, 2000).
[45]L. Berger, A. Attili, M. Gauding, and H. Pitsch, "Effects of Karlovitz number variations on thermodiffusive instabilities in lean turbulent hydrogen jet flames," Proc. Combust. Inst. **40**, 105219 (2024).
[46]L. Berger, M. Grinberg, B. Jürgens, P. E. Lapenna, F. Creta, A. Attili, and H. Pitsch, "Flame fingers and interactions of hydrodynamic and thermodiffusive instabilities in laminar lean hydrogen flames," Proc. Combust. Inst. **39**, 1525–1534 (2023).
[47]T. A. Butcher and J. M. D. Coey, "Magnetic forces in paramagnetic fluids," J. Phys.: Condens. Matter **35**, 053002 (2023).
[48]A. C. Kruse, P. G. Aleiferis, and A. Giusti, "Numerical investigation of the effect of a magnetic field on the transport of oxygen in air," Phys. Fluids **38**, 057112 (2026).

02 October 2026 08:40:23

© Author(s) 2026